An evaluation of mass-normalization using 50th and 95th percentile human body finite element models in frontal crash

Matthew L. Davis, Nicholas A. Vavalle, and F. Scott Gayzik

Abstract Human body finite element models (FEMs) are ideal tools to explore the effects of body habitus on the biomechanical response of a given subject in a vehicle crash. This study aims to investigate the differences between a large male (M95) FEM and an average male (M50). The models are identical aside from their respective morphologies. The same generic frontal crash driver-side buck was used with each model with an acceleration pulse from a late model NCAP crash. The HIC_{15} of the M50 and M95 models were 491 and 806. The Brain Injury Criteria values for the M50 and M95 models were 0.50 and 0.64, respectively. Neck Injury Criteria for the M50 and M95 models were 0.44 and 0.41, respectively. The percent chest deflections were 21.1% for M50 and 17.3% for M95. Equal stress, equal velocity scaling was used to scale M95 outputs to the M50. Mass scaling was found to increase correlation of signal phases, but had diminished effect on magnitude and shape. Given the global trend of increased size of occupants, this study provides insight into the effects of body habitus on the occupant kinematics and injury risk in frontal crash.

Keywords Finite Element (FE), Human Body Modelling (HBM), injury biomechanics, large male, model morphing.

I. INTRODUCTION

According to the United States Census Bureau, there are approximately 113 million adult males in the USA [1], meaning that there are over 5 million that are at least the 95th percentile stature. This segment of the population is under-represented in the United States New Car Assessment Program (US NCAP); currently, no 95^{th} percentile male anthropometric test devices (ATDs) are included in the protocols. Further, the USA adult population increased in both height (3 cm increase) and weight (11 kg increase) between 1960 and 2002 [2]. It has been shown that tall occupants can be left unprotected by side airbag systems and can strike the vehicle structure instead of the airbag [3]. This study aims to present injury risk differences between an average male and large male, using two validated human body finite element models (FEMs) in an identical simulated crash condition.

Two models from the Global Human Body Models Consortium (GHBMC) were used in this study – the average male model (M50) and the large male model (M95). A regional model approach was used in the development and validation of the M50 model. Head [4-6], neck [7-10], thorax [11,12], abdomen [13], pelvis [14] and lower extremity [15-17] models were developed and validated by consortium universities and were then integrated into one full body model [18-22]. The full body M95 model was morphed from the M50 model and was subsequently validated in 7 conditions [23].

The objective of the current study is to evaluate the effects of body habitus on the outcomes of a representative consumer crash test. Both the M50 and M95 were simulated in a simplified driver buck designed for frontal impacts with a United States New Car Assessment Program (US NCAP) acceleration applied. The effects of body habitus were tested in several ways, including kinematic response and injury risk assessment.

M. L. Davis is a Graduate Student, N. A. Vavalle is a Graduate Student and F. S. Gayzik (tel: 336-716-6643, fax: 336-716-5491, e-mail: sgayzik@wakehealth.edu) is an Assistant Professor in Biomedical Engineering at Virginia Tech – Wake Forest School of Biomedical Engineering and Sciences and the Wake Forest School of Medicine in Winston-Salem, NC.

.

Finally, a quantitative curve comparison was done to evaluate how closely the response of the models matched after scaling.

However, due to the stature and weight differences between the M50 and M95 models, measured variables from simulations must be normalized to a reference (in this case, the M50). Two common approaches for obtaining normalized and scaled response data are the impulse-momentum [24] and equal-stress equal-velocity (ESEV) methods [25,26]. The impulse-momentum method takes into account the type of test and effective mass and length characteristics of specific body regions involved. Because of this, the impulse momentum is considered to be a more specific evaluation than ESEV. However, the ESEV method relies only on the mass ratio between the M50 and the M95. As such, this approach is applied in the current study, because all body regions in this case are coupled. ESEV sidesteps the potential error which could be introduced when determining effective masses and characteristic lengths of coupled body regions.

II. METHODS

A. Human Body Models

The Global Human Body Models Consortium (GHBMC) average male (M50) [20,21,27] and large male (M95) [23] LS-Dyna (971 R6.1.1, LSTC, Livermore, CA) models were used for this study. For both models, target stature and weight values were determined by those used in development of the M50 and M95 Hybrid III ATDs. The development approach for the M50 model can be found in the literature [28], but briefly, a multi-modality approach was used to collect imaging data of a living subject and subsequently made into CAD. The imaging approach leveraged the strengths of MRI, upright MRI, CT and external laser scanning to obtain highly detailed information of the subject in a seated posture. The CAD was delivered to collaborating universities where regional meshing and development was completed. The full body model was integrated from the five regional models and validated for mass distribution [21] and simulation responses [20,27], in addition to the regional validation that was performed by each university [4,7,11,29,30]. In total, the average male model is composed of 1.3 million nodes, 2.2 million elements and 984 parts and represents a weight of 76.8 kg and height of 174.9 cm.

The large male model was morphed directly from the average male model using a radial basis function interpolation with a thin-plate spline basis function and relaxation algorithm (RBF-TPS) [23]. The method smoothly interpolates between a reference geometry and target geometry using a relatively reduced set of landmarks across the whole body [31,32]. The RBF-TPS method required homologous landmarks on the reference (M50) and target (M95) geometries and the FE nodal locations of the reference model. The imaging data of both subjects were leveraged to acquire the input landmarks. For the development of the M95, homologous landmarks were established on the outer flesh and select abdominal organs (liver, kidneys, and spleen) of both the M50 and M95 to accurately capture the external anthropometry of the model while also representing the internal anatomy of the M95. Spline equation coefficients were calculated from the homologous landmarks and applied to the reference nodal locations to determine the target nodal locations. The relaxation algorithm was applied to improve element quality by eliminating the requirement that the spline functions pass through the landmarks. Anthropometric and anatomical verifications were performed to ensure that the relaxation did not hinder model fidelity to the target population size. The application of the RBF-TPS method produced a model that was not just a scaled version of the average male, but rather one that matched anthropometric and anatomical targets of a large male. One advantage of this morphing method is that the target model contains the same number of nodes, elements and parts as the reference model. All other modelling considerations also remained the same between the two models, but the M95 model represents a mass of 103.3 kg and stature of 189.5 cm. Direct comparisons between the models were facilitated since any given node in one model was in a homologous location on the other model.

B. Simulation

A simplified driver-side frontal crash buck design was used in this study. The buck contained several important features to allow for a reasonable approximation of a vehicle interior. The seat was modelled using a low density foam material property (density = 4.06e-8 kg/mm^3, elastic modulus = 3.05e-2 GPa, and stress strain curve, nominally 11.3 KPa at 50% strain) with a shell coating of fabric material. The knee bolster also used a low density foam material property with discrete elements connected to the buck structure to tune the response. The airbag used in the model was a hybrid jetting type that fired 6 ms after the start of the crash event. Nitrogen gas was used to inflate the bag which was modeled with a fabric material (0.55 GPa modulus, fabric thickness 0.3 mm). The mass flow rate of gas into the airbag was determined empirically and provided by the GHBMC. At its fully inflated state, the bag had a radius of 540 mm. Delta-V values of the simulated crashes were in the range indicating the use of a Stage 1+2 bag [33]. The belt stiffness was equivalent to 10 kN of force at 5.23% strain and included a pretensioner that fired 9 ms after the start of the event and a retractor that fired 17 ms after the start of the event. Further, the shoulder-belt force was limited to 3.75 kN with a force-limiter. No changes were made to the restraint system parameters for the large male model.

The acceleration pulse applied to this buck was derived from the floor accelerometer of the US NCAP test #7147 [34]. The pulse was applied to the rigid floor of the buck and prescribed motion in the three linear degrees of freedom (DOF) with constraints applied for rotational degrees of freedom. The test was a frontal crash test into a barrier at 56.2 km/h. The total delta-v of this impact was 65.6 km/h, as seen in the velocity profile of the simulation in Fig. 1.

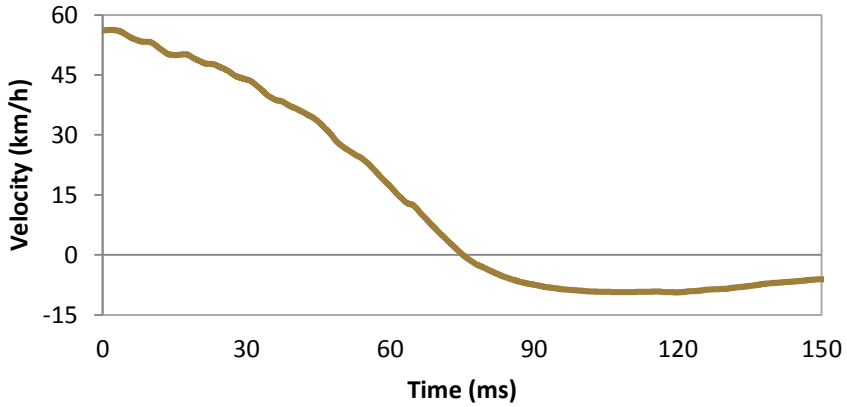

Fig. 1. Velocity profile in NCAP Test #7147, integrated from the acceleration that was used as the simulation boundary condition.

To accommodate the size of the M95 model the seat was moved rearward by 145 mm and downward by 39.5 mm. For both simulations the models were settled into the seat, using gravity, for 100 ms. The belt was subsequently fitted on the settled model using the built-in belt-fitting capabilities of LS-PrePost v4.2 (LSTC, Livermore, CA). The crash event was then simulated to 150 ms.

All simulations were computed using LS-Dyna v6.1.1 MPP (LSTC, Livermore, CA). The Wake Forest University Distributed Environment for Academic Computing (DEAC), a heterogeneous Linux-based high-performance computing system, was used. Both models were simulated on 48 processors.

C. Model Output Methods

Head accelerations were obtained from the kinematics of the skull using the history function in LS-PrePost. Head rotational velocities from the models were collected using a constrained interpolation method. A node at the centre of gravity (CG) of the head was constrained to nine nodes on the skull using the *CONSTRAINED_INTERPOLATION card in LS-Dyna. This allowed for a deformable skull that was capable of constraining the CG node. Other constraint methods typically require a rigid body. A cross-section plane at the

occipital condyles (OCs) was used to obtain neck forces and moments [35]. To calculate chest deflections, nodal coordinates were taken on a node of the sternum and a node of the T8 spinous process. These were then subtracted to obtain deflections, and normalised by the initial value to give percent deflections. Femur forces were obtained using cross-section sets that were approximately 2/3 of the length from the proximal femur to the distal femur. All outputs were obtained in local coordinate systems commensurate with the SAE J211 standards [36]. The trajectories of the inboard (right) side of the models relative to the buck were tracked by averaging a cluster of five nodes at each of the head, shoulder and hip, which are representative of typical kinematic marker locations.

Several measurements were taken from the interactions between the human body models and vehicle structure, as well. The belt forces at the upper shoulder and outer lap-belt locations were taken from the seatbelt element force outputs. The upper shoulder-belts were force-limited in both cases, and this output was used to confirm the function of this feature. The forces between the airbag and the body were examined using the contact forces. Finally, the distance between a node on the forehead and a node on the top of the steering wheel was measured.

D. Injury Risk Evaluation

For both models, a quantitative injury risk assessment was performed for individual body regions based on injury risk criteria in the literature. These values were also used to evaluate the effect of body habitus on potential injury outcomes in an otherwise identical sled pulse. For the head, neck and lower extremity regions, data were obtained using the accelerometer and section-plane techniques described above.

Head injury risk was evaluated by applying two techniques that utilised different model outputs. Existing regulations from the National Highway Traffic Safety Administration (NHTSA) specify performance limits for a Head Injury Criteria (HIC) [37-39]. An industry standard, HIC_{15} is a measure of the maximum average translational acceleration over any 15 ms duration of an impact event. All outputs used in the calculation of HIC_{15} scores were obtained from acceleration of the head CG node of both the M50 and M95 models. Head injury risk was also evaluated using the Brain Injury Criteria (BrIC) developed by Takhounts et al. [5]. This injury criterion differs from HIC in that prediction is not based on acceleration data. Instead, prediction is determined by the directional dependence of maximum angular velocities. To calculate BrIC for both models, angular velocity data was obtained from the head CG node that used the constrained interpolation method.

Neck injury risk was assessed using the Neck Injury Criteria (Nij). Nij is evaluated by linearly combining the normalised axial load and normalised flexion/extension moment about the occipital condyle [37,40]. In both axial load and moments, the critical neck intercept values used for normalisation were applied per the suggested values for the M50 and M95. Axial load and neck moment data were obtained from the section plane placed at the occipital condyle to mimic data acquisition from ATD tests.

The risks of injury to thoracic structures in the models were evaluated using two displacement criteria. The first was the compression criteria established by Kroell et al. [41]. The compression criterion is a linear equation that uses maximum chest compression percentage as a predictor for the level of AIS severity. Here, chest compression is calculated by the maximum chest displacement divided by initial chest depth. The second method used for evaluation was the chest deflection criteria, where maximum chest deflection was related to AIS injury risk based on risk curve equations used in the US NCAP [42-44].

As the M50 and M95 models were simulated in a frontal sled pulse with knee contact to the bolster, femur tolerance loads were used to assess risk of injury to the lower extremity. These values were obtained from the models using section planes in the femur corresponding to the location of data acquisition in ATDs [37]. To use the M95 data in the injury risk equation, femur loads from that model were scaled by the femur cross-sectional area scale factor established by Mertz et al. [45]. M50 data were not scaled since the injury risk equation was developed for an average male.

E. ISO Comparison with Eppinger Scaling

Part of ISO/TS 18571, a technical standard regarding the quantitative assessment of dynamic data, was used to quantitatively compare the model output curves. The standard uses a weighted average of four metrics – corridor, phase, magnitude and slope – to derive a total score describing the fit of data to a reference curve. Scores can range from 0 to 1, with 1 being the best. The score is categorised into excellent, good, fair, or poor Total ISO Ratings, based on the thresholds 0.94, 0.80 and 0.58, respectively. For the purposes of this study, only the phase, magnitude and slope scores were calculated. Further explanation of this is included within the discussion section.

The phase, magnitude and slope scores are calculated using the methods of Enhanced Error Assessment of Time Histories (EEARTH) [46], which compares a model curve to a single reference curve. The phase score uses the time shift of the maximum cross correlation in a linear regression. Zero time shift receives a phase score of 1 and the maximum allowable time shift of 20% receives a phase score of 0. The magnitude and slope scores are calculated from the time-shifted data. Dynamic time warping (DTW) is used in calculating the magnitude score to parse out the effects of phase on magnitude differences. The one-norm of the difference between the shifted and warped curves are calculated for each time point and normalised by the one-norm of the shifted and warped reference curve. The magnitude score is calculated using a linear regression between no difference (magnitude score 1) and a maximum allowable difference of 0.5 (magnitude score 0). The slope score is calculated from the time-shifted data without DTW applied, since DTW compromises the time-dependence of slope. The average slope is calculated in 1 ms intervals and the same one-norm procedure used for the magnitude calculation is performed. The slope score is calculated as the linear regression between zero difference (slope score 1) and a maximum allowable difference of 2.0 (slope score 0).

Typically, the reference curves represent average experimental data and the curves being assessed are from a model or ATD. However, in the case of this study, the reference curves were the M50 model data and the M95 model data were being assessed. The M95 data were scaled to the M50 data using the ESEV methods developed by Eppinger [25]. This approach assumes linear relationships among time, length, and mass (Equations 1-3), where T is the unit of time, L is the unit of length, and M is the unit of mass.

$$T_{M50} = \lambda_t T_{M95} \quad (1)$$

$$L_{M50} = \lambda_l L_{M95} \quad (2)$$

$$M_{M50} = \lambda_m M_{M95} \quad (3)$$

ESEV also assumes that both models have identical density and modulus of elasticity. By applying these assumptions, and substituting equations 1-3 into the functions for density and elastic modulus, normalization factors can be found for time, deflection, acceleration, force, and moment (Equations 4-8). Full derivation of these normalization factors can be found in the literature [25,26].

$$Time\ Normalization\ Factor = \lambda^{\frac{1}{3}} \quad (4)$$

$$Deflection\ Normalization\ Factor = \lambda^{\frac{1}{3}} \quad (5)$$

$$Acceleration\ Normalization\ Factor = \lambda^{\frac{-1}{3}} \quad (6)$$

$$Force\ Normalization\ Factor = \lambda^{\frac{2}{3}} \quad (7)$$

$$Moment\ Normalization\ Factor = \lambda \quad (8)$$

In order to make observations on the efficacy of mass scaling between these models, the ISO comparison was made between unscaled M95 data to M50 as well as scaled M95 data to M50, with the unscaled data acting as a baseline against which the scaled scores were compared. The head accelerations (x, y and z), neck axial force, neck flexion/extension moment, chest deflection, and left and right femur forces were compared using this method. The hypothesis was that, after mass scaling, model responses would be improved as compared to before scaling and would be closer to scores of 1.

III. RESULTS

Both models completed the simulation without numerical error. The peak hourglass energy, as a percentage of the internal energy and total simulation energy, was 7.3% and 0.5% in the M50 simulation and 12.0% and 1.0% in the M95 simulation. Hourglass energies were also observed on a part by part basis, and largest contributors were shown to be stable in the model [47]. Further, there were no discontinuities in the hourglass energy curve throughout either simulation. Discontinuities in this curve can be indicative of a numerical instability.

A. Kinematics

The simulations can be seen in Fig. 2, where time-lapse images of both models in the crash event are included. The trends of the model responses appear similar, with the exception that the additional mass of the M95 brings the model further towards the steering column, increasing the load on the airbag. This is confirmed in the contact forces between the airbag and body, where the peak of the M50 is 8.3 kN and the peak of the M95 is 9.2 kN. While the shoulder-belt forces were held constant by the force-limiter, the lap-belt forces between the two models differed. The peak lap-belt force in the M50 model was 6.6 kN, whereas the peak in the M95 model was 9.1 kN. A graph showing the restraint force information is shown in Fig. 3.

	M50	M95
t=0	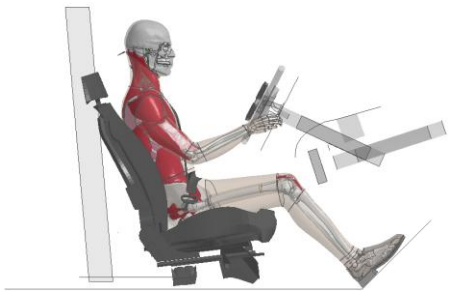	
$t=\frac{1}{4}t_{final}$	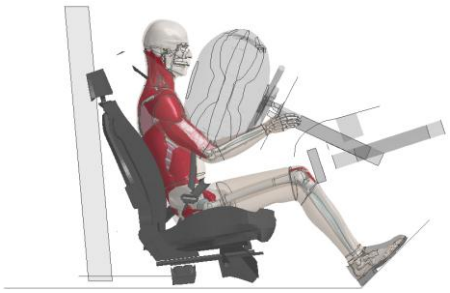	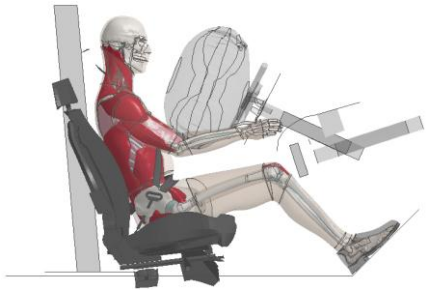
$t=\frac{1}{2}t_{final}$	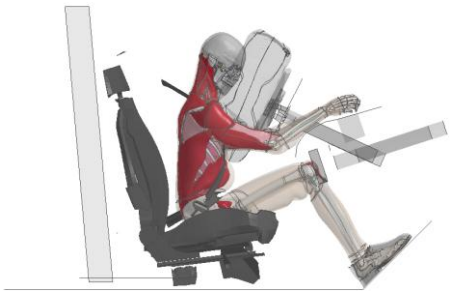	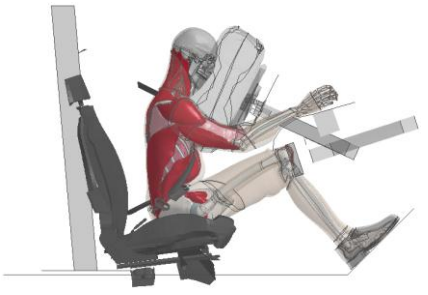
$t=\frac{3}{4}t_{final}$	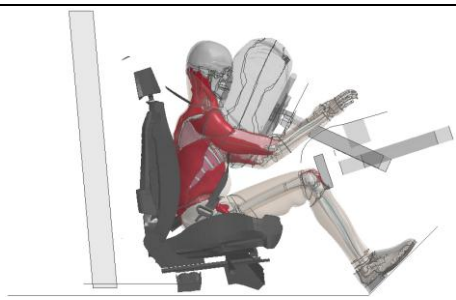	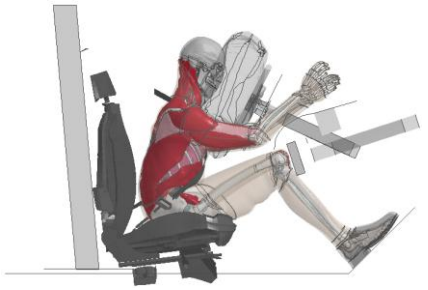
$t=t_{final}$	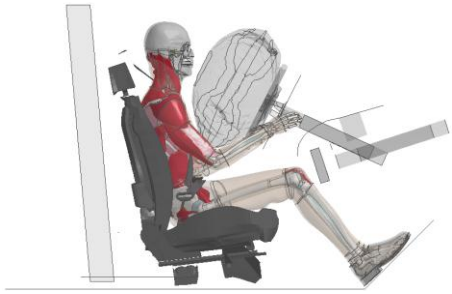	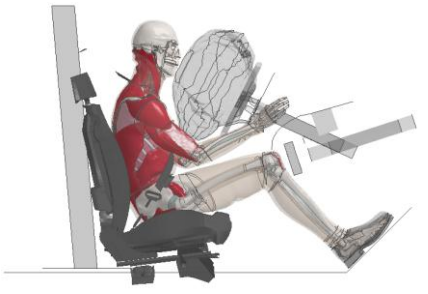

Fig. 2. Time-lapse images of the M50 and the M95 in the frontal NCAP simulation.

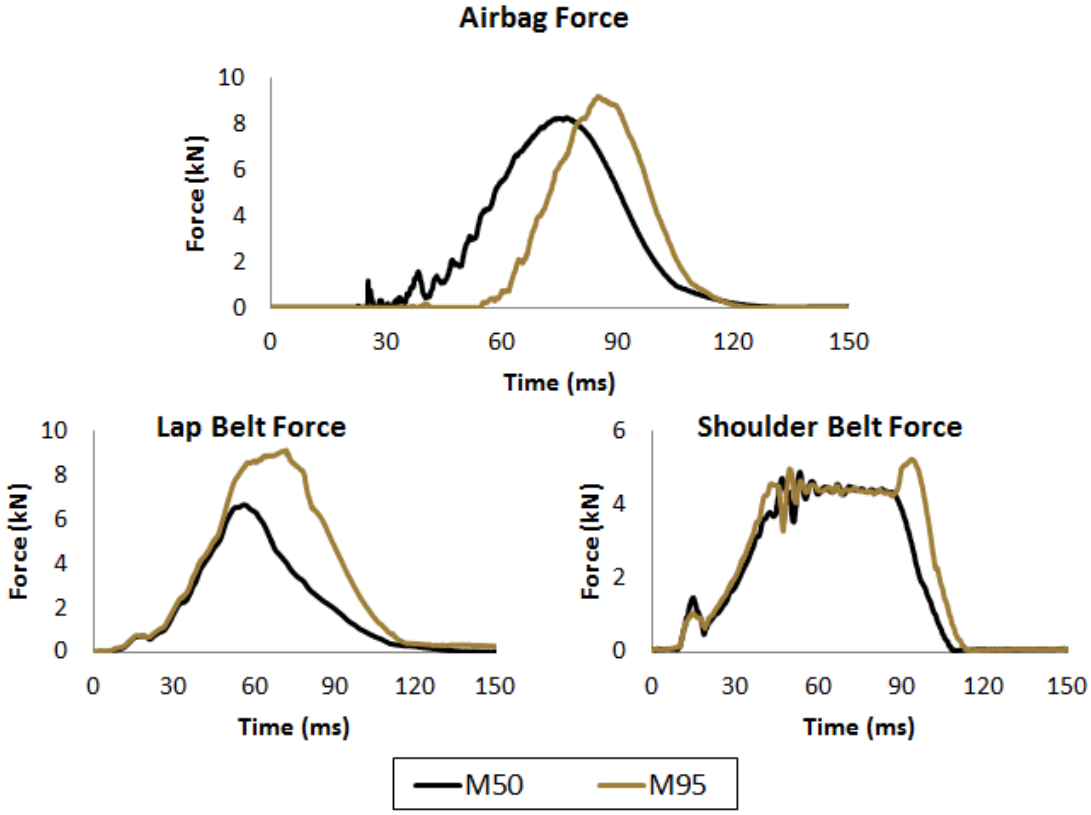

Fig. 3. Restraint force data from the M50 and M95 models. Airbag forces are plotted on the left, while belt forces are plotted on the right.

The trajectories of the head, shoulder and hip were found to differ between the two models, as seen in Fig. 4. In all three locations the M95 model displayed greater forward motion than the M50 model. The total magnitude of forward excursion was found to be less in the hip area, which was restrained by the seat and lap-belt. The head displacement in the X direction was 154.3% greater in the M95 and the shoulder displacement was 139.5% greater. In the hip, the X direction motion of the M95 was139.9% greater than the M50. The total Z motion in the hip was the smallest gross displacement of any of the regions for both models. To shed light on possible injury risk, the relative distance between the head of the models and the steering wheel was also observed. The distance between a homologous node on the forehead of each model and the top of the steering wheel was measured. The M95 model started approximately 125 mm further from the wheel than the M50 model and, at its closest, was 49.6 mm closer. This can be seen in Fig. 5.

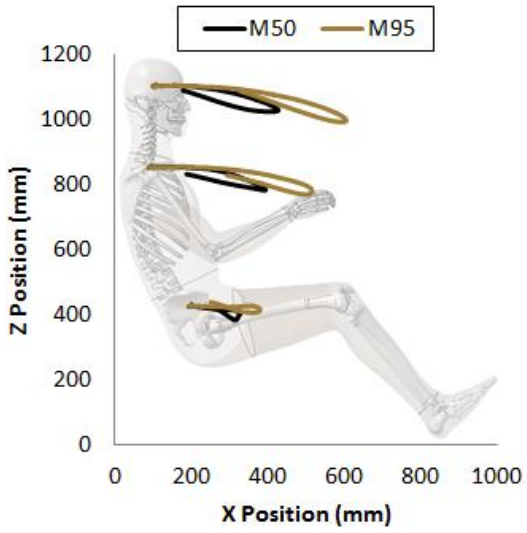

Fig. 4. Head, shoulder and hip trajectories of the average and large male for the duration of the simulation.

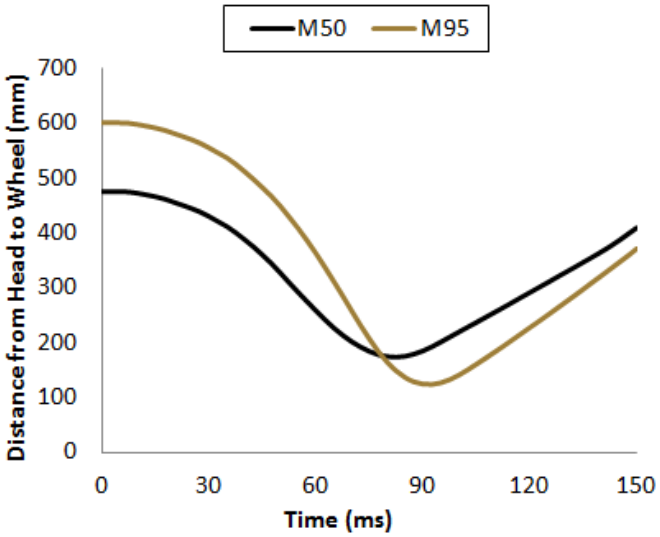

Fig. 5. Distance from the forehead of each model to the top of the steering wheel.

B. Injury Risk

The HIC_{15} of the M50 and M95 models were 491 and 806, respectively, with corresponding injury risk values included in Table 1. This equates to a HIC_{15} that is roughly 1.6 times larger in the M95 model than the M50 model. The value for the M95 was also above the suggested HIC_{15} performance limit of 700. The BrIC values for the M50 and M95 models were 0.50 and 0.64, respectively. Nij values for the M50 and M95 models were 0.44 and 0.41, respectively, which in both cases is below the performance limit of 1.0. In both the M50 and M95, the appropriate critical intercepts were used to account for the difference in body habitus. The percent chest deflections were 21.1% for M50 and 17.3% for M95, lower for the larger model. Based on these values, the chest compression criterion predicts an AIS injury level of 1 for both the M50 and M95. Within Table 1, injury probability to the thorax can be seen in terms of peak chest deflection. Peak femur forces for the left and right leg in the M50 model were 4.1 kN and 6.7 kN, while they were 6.0 kN and 6.9 kN in the M95 model. The largest difference was seen in the HIC_{15} values of the models. Data on the probability of injury for the head, neck, thorax and lower extremity can be seen in Table 1.

TABLE 1
INJURY RISK COMPARISON BY BODY REGION

Criteria	M50			M95		
	Model Value	Threshold	P(AIS3+)	Model Value	Threshold	P(AIS3+)
HIC_{15}	491.3	700	4.5%	805.5	700	15.2%
Nij	0.44	1.0	8.6%	0.41	1.0	8.2%
Thoracic Chest Deflection (mm)	36.9	63	12.4%	31.6	70	8.7%
Femur Force, Left (kN)	4.1	10.0	2.6%	6.0	12.7	3.1%
Femur Force, Right (kN)	6.7	10.0	5.8%	6.9	12.7	3.9%

C. ISO Comparison

The ISO/TS 18571 comparison, with corridor scores omitted, can be seen in Table 2, with both the native M95 data, as a baseline, and mass scaled M95 data. Overall, the scaled M95 data received scores that would have been commensurate with fair ratings given the full complement of ISO standard scoring. On average, mass scaling had the largest effect on the phase score, improving the average value by 0.13. The slope score was

improved by 0.08. Mass scaling was found to have the least effect on the magnitude score. The highest scores tended to be in the mass scaled phase correlations, which ranged from 0.73 to 1.00. The magnitude scores were in the middle of the three scores, on average, with a range of 0.00 to 0.79. The outlier in this group was the hip z displacement, which received the only 0.00 score out of any of the categories and was 0.56 below the next lowest magnitude score. Also, gross Z motion (upwards or downwards) was constrained by the seat- and lap-belt, and was small in comparison to the fore-aft direction. The lowest scores, on average, occurred on the slope, which ranged from 0.21 to 0.79.

TABLE 2

ISO/TS 18571 COMPARISON BETWEEN THE MODELS. FOR THE PURPOSES OF THIS COMPARISON, ALL M95 DATA LABELLED AS SCALED WERE DONE SO USING THE EPPINGER METHOD, WHERE λ=0.74 (M50 = 76.8 KG / M95 = 103.3 KG)

Signal	Phase Score		Magnitude Score		Slope Score	
	Unscaled M95	Scaled M95	Unscaled M95	Scaled M95	Unscaled M95	Scaled M95
Head CG Accel. X	0.64	0.90	0.89	0.93	0.28	0.41
Head CG Accel. Y	0.92	0.80	0.62	0.56	0.22	0.26
Head CG Accel. Z	0.66	0.88	0.68	0.70	0.32	0.30
Neck Force Axial	0.60	1.00	0.93	0.80	0.61	0.64
Neck Flex./Ext. Moment	0.80	0.98	0.78	0.68	0.55	0.64
Chest Deflection	0.94	0.73	0.57	0.63	0.75	0.77
Hip X Displacement	0.82	0.93	0.61	0.82	0.77	0.79
Hip Z Displacement	0.78	0.90	0.00	0.00	0.75	0.76
Left Femur Force	0.83	0.97	0.77	0.82	0.01	0.21
Right Femur Force	0.81	1.00	0.79	0.68	0.14	0.39

IV. DISCUSSION

The GHBMC average male and large male models were compared in a frontal US NCAP simulation. A simplified driver-side buck was used in the study to apply the crash pulse collected from US NCAP test #7147 in the NHTSA Online Database. The pulse and buck were identical between simulations, the only difference being the human body model and seat position. Since the M95 was morphed from the M50, this study focuses on the effect of this morphing on full body kinematics and injury risk.

The models displayed differences in outputs and injury risks, with the M95 model at an increased risk for injury to the head. A number of factors related to the size and stature differences between models led to these findings. The additional mass provided by the large male model accounted for a 9.2% increase in peak kinetic energy within the system. Increased stature required a more rearward seat track for the M95 model. Thus, inflation of the airbag occurred prior to model contact in the case of the M95. In comparison, the M95 contacted the airbag 54 ms into the simulation, whereas the M50 model made contact at 30 ms. The proximity

of the chest to the airbag in the M50 model likely contributed to the larger chest deflection, and therefore injury risk observed. The distance of the M95 model from the airbag, coupled with the force limiting belt, led to more forward excursion before loading the countermeasures, yielding a shorter duration loading pulse (Fig. 3). This shorter time of engagement increased forward head excursion (Figs 4 and 5; Table 1) and led to greater linear and rotational head acceleration, as evidenced by increases in HIC and BrIC. Also, the M95 experienced knee bolster impact prior to engaging the airbag (44.5 ms), which may have contributed to the increase in forward excursion of the head and shoulders. While knee bolster contact happened prior to airbag engagement for the M95, the M50 model struck the knee bolster earlier in the simulation (37.5 ms) because of its initial position closer to the wheel. Also, due to adjustments made to seat position, both models had similar locations of engagement with the airbag and knee bolster.

The model curves were shown to be quantitatively different through the use of ISO/TS 18571, a recently released standard for quantitative assessment of dynamic data sets. The M95 model is a morphed version of the M50 model. As such, these models lend themselves to investigating mass scaling effects since two assumptions of Eppinger's method are perfectly held: that the reference and target subjects have the same modulus and density. No material model adjustments were made after morphing the M95 model, only nodal locations are different between the two models. Regarding the assumption of geometric similitude, the M95 is not an exact scaled version of M50 but morphed to match a typical 95th percentile male subject. However, the similitude is thought to be on par with PMHS subjects, and this mass scaling method is widely applied despite subject-to-subject variability. Given the arguments above, the ISO comparison could be regarded as an examination of the geometric similitude assumption. However, the fixed size of the buck is a confounding factor in this study, since the larger model interacted at different times and durations with the countermeasures, potentially altering the time histories in ways that scaling alone could not account for (as seen in the hip kinematics). Despite that limitation, mass scaling increased the quantitative comparison scores between models. Ideally, a mass scaling method would yield ISO scores approaching 1, with the target model (M50, in this study). The results indicated that scaling had the greatest effect on phase, with smaller effects seen on magnitude and shape. However, *post hoc* scaling of data is, in itself, a model with assumptions and approximations. Future work will focus on using this approach to more closely evaluate the relative pros and cons of scaling techniques.

The full ISO/TS 18571 comparison uses constant-width corridors as a means of considering subject-to-subject variability. The corridor score was not included in this analysis since model outcomes are deterministic and variability would not be expected. Because of this, total ISO Scores and their corresponding ISO Ratings were not assigned to the curve comparisons.

The study was also limited in that vehicle deformation was not considered. A deceleration pulse was applied to the floor of the buck without the application of floor pan intrusion or potential effects on the steering column. For example, from the report of this NCAP test, the brake pedal was 50 mm closer to the front of the seat track in post-crash measurements and the centre of the steering-wheel hub was 11 mm closer. Future work could focus on full vehicle crash simulations with the human body models included, to explore the effects of body habitus on injury risk in a more real-world setting.

V. CONCLUSIONS

This work presented a comparative study between an average male and a large male human body finite elements model. The models were simulated in a US NCAP frontal impact test and biomechanical data and injury risks were evaluated. Significant differences were found between the models, with the large male at a higher risk for head injury and slightly lower risk for chest injury. Quantitative comparison methods were used, to assess the efficacy of mass scaling methods. Equal stress, equal velocity mass scaling resulted in modest gains in curve comparison, on average, providing a fair response match. The mass scaling was found to have the greatest impact on reducing phase differences between models. These models can be leveraged within the

injury biomechanics community to better understand the effects of body habitus on injury risk and design safety features tailored to larger occupants.

VI. ACKNOWLEDGEMENTS

The authors would like to acknowledge the Global Human Body Models Consortium, LLC, for funding and support. Wake Forest University is the Integration Center of Expertise of the Global Human Body Models Consortium. The authors gratefully acknowledge the meshing and validation efforts by our academic partners in the GHBMC, including King Yang and Liying Zhang (Wayne State U., USA), Duane Cronin (U. Waterloo, Canada), Richard Kent, Damien Subit and Matt Panzer (U. Virginia, USA), Philippe Beillas (IFSTARR, France), Warren Hardy (Virginia Tech, USA), Costin Untaroiu and Jeff Crandall (U. Virginia, USA), and Alan Eberhardt (U. Alabama Birmingham, USA). The abdominal impact deflection method was developed by Philippe Beillas. All simulations were run on the DEAC cluster at Wake Forest University, with support provided by Drs. Damian Valles and Timothy Miller.

VII. REFERENCES

[1] "Current Population Survey, Annual Social and Economic Supplement." United States Census Bureau December 2013.
[2] Ogden C., Fryar C., Carroll M. and Flegal K. "Mean body weight, height, and body mass index, United States 1960-2002." National Center for Health Statistics, Hyattsville, MD 2004.
[3] Loftis K. L., Weaver A. A. and Stitzel J. D. Investigating the Effects of Side Airbag Deployment in Real-World Crashes Using Crash Comparison Techniques. Annals of Advances in Automotive Medicine / Annual Scientific Conference*, 2011,* vol. 55: pp. 81-90.
[4] Mao H., Zhang L., et al. Development of a Finite Element Human Head Model Partially Validated With Thirty Five Experimental Cases. Journal of biomechanical engineering*, 2013,* vol. 135: p. 111002.
[5] Takhounts E. G., Craig M. J., Moorhouse K., McFadden J. and Hasija V. Development of Brain Injury Criteria (BrIC). Stapp car crash journal*, 2013,* vol. 57: pp. 243-266.
[6] Yanaoka T. and Dokko Y. "A Parametric Study of Age-Related Factors Affecting Intracranial Responses under Impact Loading Using a Human Head/Brain FE Model." in *International Research Council on Biomechanics Injury (IRCOBI)* Gothenburg, Sweeden, 2013.
[7] DeWit J. A. and Cronin D. S. Cervical Spine Segment Finite Element Model for Traumatic Injury Prediction. Journal of the Mechanical Behavior of Biomedical Materials*, 2012,* vol. 10: pp. 138-150.
[8] Fice J. B., Cronin D. S. and Panzer M. B. Cervical spine model to predict capsular ligament response in rear impact. Annals of biomedical engineering*, 2011,* vol. 39: pp. 2152-2162.
[9] Mattucci S. F., Moulton J. A., Chandrashekar N. and Cronin D. S. Strain rate dependent properties of younger human cervical spine ligaments. Journal of the mechanical behavior of biomedical materials*, 2012,* vol. 10: pp. 216-226.
[10] Mattucci S. F., Moulton J. A., Chandrashekar N. and Cronin D. S. Strain rate dependent properties of human craniovertebral ligaments. Journal of the mechanical behavior of biomedical materials*, 2013,* vol. 23: pp. 71-79.
[11] Li Z., Kindig M. W., et al. Rib Fractures Under Anterior-Posterior Dynamic Loads: Experimental and Finite-Element Study. Journal of Biomechanics*, 2010,* vol. 43: p. 228.234.
[12] Li Z., Kindig M. W., Subit D. and Kent R. W. Influence of mesh density, cortical thickness and material properties on human rib fracture prediction. Medical engineering & physics*, 2010,* vol. 32: pp. 998-1008.
[13] Soni A. and Beillas P. Modelling hollow organs for impact conditions: a simplified case study. Comput Methods Biomech Biomed Engin*, 2013,* vol. [Epub ahead of print]:
[14] Kim Y. H., Kim J. E. and Eberhardt A. W. A new cortical thickness mapping method with application to an in vivo finite element model. Comput Methods Biomech Biomed Engin*, 2012,* vol. 17: pp. 997-1001.
[15] Shin J. and Untaroiu C. Biomechanical and Injury Response of Human Foot and Ankle under Complex Loading. J Biomech Eng*, 2013,* vol. 135:
[16] Untaroiu C. D., Yue N. and Shin J. A finite element model of the lower limb for simulating automotive impacts. Ann Biomed Eng*, 2013,* vol. 41: pp. 513-26.
[17] Yue N. and Untaroiu C. D. A numerical investigation on the variation in hip injury tolerance with occupant posture during frontal collisions. Traffic Injury Prevention*, 2014,* vol. 15: pp. 513-522.

[18] Hayes A. R., Vavalle N. A., Moreno D. P., Stitzel J. D. and Gayzik F. S. Validation of simulated chestband data in frontal and lateral loading using a human body finite element model. Traffic injury prevention*, 2014,* vol. 15: pp. 181-186.
[19] Vavalle N. A., Jelen B. C., Moreno D. P., Stitzel J. D. and Gayzik F. S. An evaluation of objective rating methods for full-body finite element model comparison to PMHS tests. Traffic Injury Prevention*, 2013,* vol. 14: pp. S87-S94.
[20] Vavalle N. A., Moreno D. P., Rhyne A. C., Stitzel J. D. and Gayzik F. S. Lateral impact validation of a geometrically accurate full body finite element model for blunt injury prediction. Ann Biomed Eng*, 2013,* vol. 41: pp. 497-512.
[21] Vavalle N. A., Thompson A. B., Hayes A. R., Moreno D. P., Stitzel J. D. and Gayzik F. S. Investigation of the Mass Distribution of a Detailed Seated Male Finite Element Model. J Appl Biomech*, 2013,* vol. [Epub ahead of print]:
[22] Park G., Kim T., Crandall J. R., Arregui-Dalmases C. and Luzon-Narro J. "Comparison of Kinematics of GHBMC to PMHS on the Side Impact Condition." in *International Research Council on Biomechanics of Injury* Gothenburg, Sweden, 2013.
[23] Vavalle N. A., Schoell S. L., Weaver A. A., Stitzel J. D. and Gayzik F. S. Application of Radial Basis Function Methods in the Development of a 95th Percentile Male Seated FEA Model. Stapp Car Crash J*, 2014,* vol. 58: pp. 361-384.
[24] Mertz H. J. "A procedure for normalizing impact response data." SAE Technical Paper 1984.
[25] Eppinger R. H. "Prediction of thoracic injuries using measurable experimental parameters." in *Proceedings of the Sixth International Technical Conference on the Enhanced Safety of Vehicles (ESV)*, 1976.
[26] Yoganandan N., Arun M. W. and Pintar F. A. Normalizing and scaling of data to derive human response corridors from impact tests. Journal of biomechanics*, 2014,* vol. 47: pp. 1749-1756.
[27] Vavalle N. A., Davis M. L., Stitzel J. D. and Gayzik F. S. Quantitative Validation of a Human Body Finite Element Model Using Rigid Body Impacts. Annals of Biomedical Engineering*, 2014,* pp. 1-12.
[28] Gayzik F. S., Moreno D. M., Geer C. P., Wuertzer S. D., Martin R. S. and Stitzel J. D. Development of a Full Body CAD Dataset for Computational Modeling: A Multi-Modality Approach. Annals of Biomedical Engineering*, 2011,* vol. 39: pp. 2568-2583.
[29] Soni A. and Beillas P. Modelling hollow organs for impact conditions: a simplified case study. Comput Methods Biomech Biomed Engin*, 2013,*
[30] Shin J., Yue N. and Untaroiu C. D. A finite element model of the foot and ankle for automotive impact applications. Ann Biomed Eng*, 2012,* vol. 40: pp. 2519-31.
[31] Bookstein F. L. Principal warps: thin-plate splines and the decomposition of deformations. IEEE*, 1989,* vol. 11: pp. 567-585.
[32] Donato G. and Belongie S. "Approximate thin plate spline mappings." in *Computer Vision—ECCV 2002*: Springer, 2002, pp. 21-31.
[33] Gabler H. C. and Hinch J. "Evaluation of Advanced Air Bag Deployment Algorithm Performance using Event Data Recorders." in *Annals of Advances in Automotive Medicine/Annual Scientific Conference*, 2008, p. 175.
[34] NHTSA. "Biomechanics Test Database: http://www-nrd.nhtsa.dot.gov/database/VSR/veh/QueryTest.aspx." Updated 2012.
[35] White N. A., Moreno D. P., Gayzik F. S. and Stitzel J. D. Cross-sectional neck response of a total human body FE model during simulated frontal and side automobile impacts. Comput Methods Biomech Biomed Engin*, 2013,* vol. [Epub ahead of print]
[36] SAE. "Instrumentation for impact test - part 1: electronic instrumentation." vol. J211/1 Warrendale, PA: Society of Automotive Engineers, 2014.
[37] Eppinger R., Sun E., et al. Development of improved injury criteria for the assessment of advanced automotive restraint systems–II. National Highway Traffic Safety Administration*, 1999,* pp. 1-70.
[38] Prasad P. and Mertz H. J. "The position of the United States delegation to the ISO Working Group 6 on the use of HIC in the automotive environment." SAE Technical Paper 1985.
[39] Mertz H. J., Prasad P. and Irwin A. L. "Injury risk curves for children and adults in frontal and rear collisions." SAE Technical Paper 1997.
[40] Prasad P. and Daniel R. P. "A biomechanical analysis of head, neck, and torso injuries to child surrogates due to sudden torso acceleration." SAE Technical Paper 1984.
[41] Kroell C., Schneider D. and Nahum A. Impact Tolerance and Response of the Human Thorax. Stapp Car Crash J*, 1971,* vol. 15:

[42] Transportation D. o. "Docket No. NHTSA-2006-26555." in *Consumer Information*, 2006.
[43] Sohr S. and Heym A. "Benefit of adaptive occupant restraint systems with focus on the new US-NCAP rating requirements." in *Proceedings: International Technical Conference on the Enhanced Safety of Vehicles*, 2009.
[44] Laituri T. R., Prasad P., Sullivan K., Frankstein M. and Thomas R. S. "Derivation and evaluation of a provisional, age-dependent, AIS3+ thoracic risk curve for belted adults in frontal impacts." SAE Technical Paper 2005.
[45] Mertz H., Irwin A., Melvin J., Stanaker R. and Beebe M. "Size, weight and biomechanical impact response requirements for adult size small female and large male dummies." SAE Technical Paper 1989.
[46] Zhan Z., Fu Y. and Yang R.-J. Enhanced Error Assessment of Response Time Histories (EEARTH) Metric and Calibration Process. Gas*, 2011,* vol. 2012: pp. 02-15.
[47] Takhounts E. G., Eppinger R. H., Campbell J. Q., Tannous R. E., Power E. D. and Shook L. S. On the Development of the SIMon Finite Element Head Model. Stapp car crash journal*, 2003,* vol. 47: pp. 107-133.